Low Resolution Picture Transmission (LRPT) Demonstration System

Phase II Report

June 20, 2002

Version: 1.0

Wai Fong
Code 564 NASA/GSFC

Pen-Shu Yeh
Code 564 NASA/GSFC

Victor Sank
QSS

Xuan Nyugen
QSS

Wei Xia
GST

Steve Duran
NASA/JSC

National Aeronautics and Space Administration
Goddard Space Flight Center
Greenbelt, MD
Code 564
Microelectronics and Signal Processing Branch

Acknowledgments

In appreciation of a special individual, the authors would like to thank the late Warner Miller whose knowledge and guidance proved immeasurable in this study. Thanks also to Jerry Weissert for his editorial assistance.

Table of Contents

Section 1: Introduction

Low-Resolution Picture Transmission (LRPT) is a proposed standard for direct broadcast transmission of satellite weather images [1]. This standard is a joint effort by the European Organization for the Exploitation of Meteorological Satellites (EUMETSAT) and the National Oceanic Atmospheric Administration (NOAA). As a digital transmission scheme, its purpose is to replace the current analog Automatic Picture Transmission (APT) system for use in the Meteorological Operational (METOP) satellites.

Goddard Space Flight Center has been tasked to build an LRPT Demonstration System (LDS). It's main objective is to develop or demonstrate the feasibility of a low-cost receiver utilizing a Personal Computer (PC) as the primary processing component and determine the performance of the protocol in the simulated Radio Frequency (RF) environment. The approach would consist of two phases. In the phase I, a Commercial-off-the-Shelf (COTS) Modulator-Demodulator (MODEM) board that would perform RF demodulation would be purchased allowing the Central Processing Unit (CPU) to perform the Consultative Committee for Space Data Systems (CCSDS) [2] protocol processing. Also since the weather images are compressed the PC would perform the decompression. Phase I was successfully demonstrated on December 1997.

Phase II consists of developing a high-fidelity receiver, transmitter and environment simulator (see Figure 1). Its goal is to find out how the METOP Specification performs in a simulated noise environment in a cost-effective receiver. The approach would be to produce a receiver using as much software as possible to perform front-end processing to take advantage of the latest high-speed PCs. Thus the COTS MODEM used in Phase I is performing RF demodulation along with data acquisition providing data to the receiving software. Also, environment simulator is produced using the noise patterns generated by Institute for Telecommunications Sciences (ITS) from their noise environment study [3].

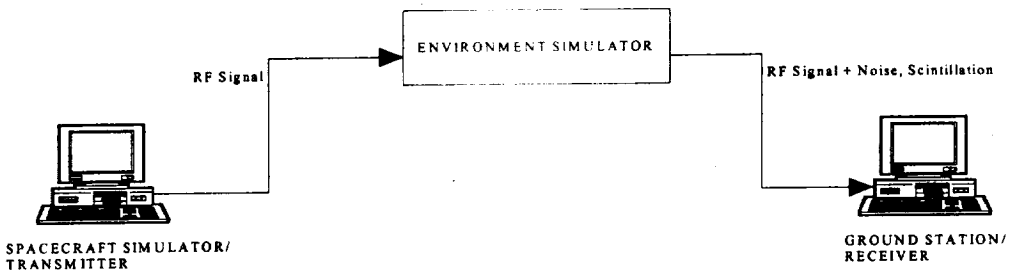

Figure 1. Phase II System Diagram

1.1 Phase II Development Plan

The goal of building a METOP compliant high-fidelity receiver presents two problems: 1. The METOP specification is an evolving document, and 2. The current proposed protocol is not available in a COTS product. As a result, an architecture that was flexible is mandatory. This necessitated the use of software to perform low-level as well as upper-level processing in the receiver. It should be pointed out that one difference between the METOP specification and the present demonstration system lies in the data compression algorithm. METOP defines the use of a modified JPEG compression scheme. Instead, the Modulated Lapped Transform (MLT) protocol is used in place of JPEG due in part to the evolving METOP specification and the availability of the MLT algorithm at GSFC.

1.2 METOP Specification Summary

This section summarizes the major points in the METOP Specification [1]. Refer to the specification for a more comprehensive treatment.

1.2.1 Application Layer

The application data defined by METOP are as follows:

- Compressed resolution imagery on selected channels of the AVHRR instrument
- Infrared and microwave sounding data from: Advanced Microwave Sounding Unit (AMSU) -A1, AMSU-A2, Microwave Humidity Sounder (MHS), and High Resolution Sounder (HIRS) instruments.
- Spacecraft Environment Monitor (SEM) data.
- Spacecraft Housekeeping data.
- GNSS Receiver for Atmospheric Sounding (GRAS) positioning and timing data.
- Administrative messages.

Data is formatted in accordance to CCSDS [2] packet Version No.1 whose structure is as follows:

<table>
<tr><td colspan="6">Packet Primary Header (48 bits)</td><td rowspan="2">Secondary Header

8 octets</td><td colspan="3" rowspan="2">User Data

Variable</td></tr>
<tr><td colspan="3">Packet Identifier

2 octets</td><td colspan="2">Packet Sequence Control
2 octets</td><td rowspan="2">Packet Length

2 octets</td></tr>
<tr><td>Version No

3 bits
"000"</td><td>Type

1 bit
"0"</td><td>Secondary Header Flag

1 bit</td><td>APID

11 bits</td><td>Sequence Flag

2 bits</td><td>Packet Sequence Count

14 bits</td><td>Time Stamp

64 bits</td><td>Ancillary Data

Var.</td><td>App. Data

Var.</td><td>Packet Error Control

16 bits</td></tr>
</table>

Figure 2. CCSDS packet Version No. 1 Format

1.2.2 Network Layer

The Network layer is represented by the path layer in the CCSDS standard. In this case, the only function of the path layer is to generate Virtual Channel Data Unit-Identifier (VCDU-id) and forward CCSDS packets to the multiplexing service.

1.2.3 Data Link Layer

The Data Link Layer receives CCSDS packets from the Network Layer and form Physical Channel Access Protocol Data Unit (PCA_PDU) to pass to the physical layer. The PCA_PDU consists of a stream of Channel Access Data Units (CADU) which are Coded Virtual Channel Data Units (CVCDU) prefixed by a Synchronization Marker. The structure of a CVCDU is shown as follows:

<table>
<tr><td colspan="6">VCDU Primary Header (6 octets)</td><td rowspan="2">VCDU Insert zone

2 octets</td><td colspan="3">VCDU Data Unit Zone</td><td rowspan="2">CVCDU Reed-Solomon Check symbols

128 octets</td></tr>
<tr><td rowspan="2">Version

"01"</td><td colspan="2">VCDU Id</td><td rowspan="2">VCDU Counter

3 octets</td><td colspan="2">Signaling Field
1 octet</td><td colspan="2">M_PDU header
2 octets</td><td rowspan="2">M_PDU Packet zone

882 octets</td></tr>
<tr><td>S/C id
8 bits</td><td>Type
6 bits</td><td>Replay flag
"0"</td><td>Spare
"0000000"</td><td>M_PDU header spare</td><td>M_PDU first header pointer</td></tr>
</table>

Figure 3. CCSDS M_PDU Format

Multiplexing Protocol Data Units (M_PDU) provide encapsulation and multiplexing for CCSDS packets.

1.2.4 Physical Layer

The METOP Specification [1] describes the functions of the physical layer as follows (refer to Figure 4):

1. Convolutional Encoding: Code rate 1/2, Constraint length 7 bits, G1=1111001/G2=1011011
2. Interleaving of the convolutionally coded signal: 36 interleaver branches, 2048 bits per elementary delay (see reference [5] for detailed description of this interleaving technique)
3. Insertion of a Unique Word (UW), 8 bits long, on every 72 bits of data for interleaving synchronization and delimitation.
4. Serial to parallel conversion
5. Modulation according to the QPSK format
6. Amplification of the modulated signal
7. Transmission from the LRPT antenna

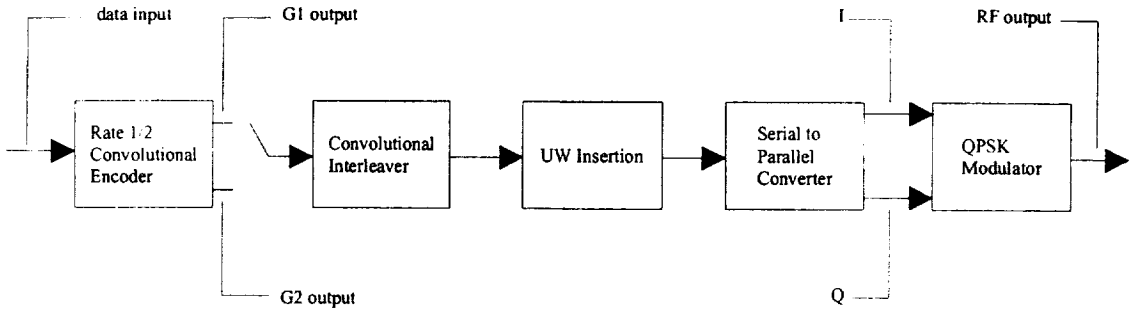

Figure 4. LRPT Modulator Block Diagram

Section 2: Transmitter System Description

The transmitter simulates the telemetry signal generated by a satellite. The block diagram is shown in Figure 5. AVHRR Image data is divided into eight scan lines stripes. Each stripe is compressed with a 10-to-1 MLT compression algorithm and placed in one CCSDS Packet. The multiplexer takes these packets and form M_PDUs. Then the M_PDUs are formatted into VCDUs and Reed-Solomon (R-S) encoded into CVCDUs with an R-S interleave depth of I=4. These CVCDUs are then made into Channel Access Data Units (CADU) by applying synchronization words and having the CCSDS recommended Bit Transition Generator applied to it. The CADUs are then convolutionally encoded and interleaved. Then, the Unique Word (UW) sync code is inserted. Finally this data stream is sent to the SEMCO MODEM where it is QPSK modulated and up-converted to 137.1 MHz. The signal is then amplified and sent to the antenna for transmission.

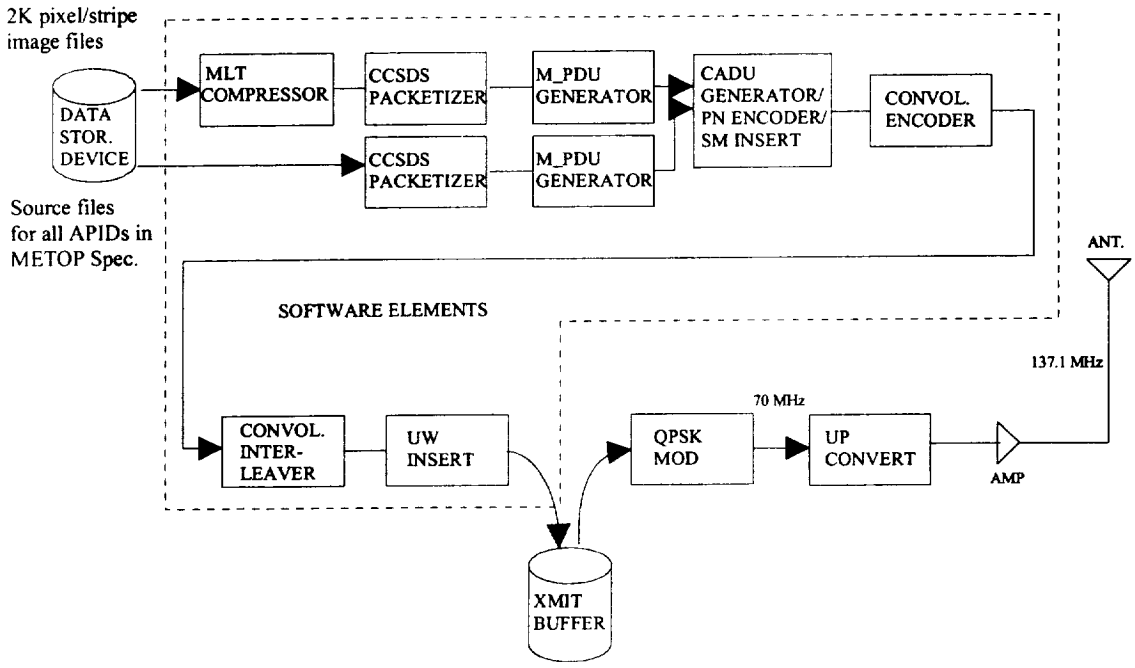

Figure 5. Transmitter Block Diagram

2.1 Transmitter Architecture and Hardware Description

Referring to Figure 6, with the exception of the upconverter, amplifier and antenna, the entire system exists in a basic PC configuration with mass storage capabilities. The image data are stored in the hard disk in the form of stripes. The stripes are read out and processed by the PC and made into CADUs and stored in the hard disk. When ready the CPU directs the CADUs to the I/O Board where the data gets converted into two serial (I and Q) streams and directed to the SEMCO MODEM. The MODEM then QPSK

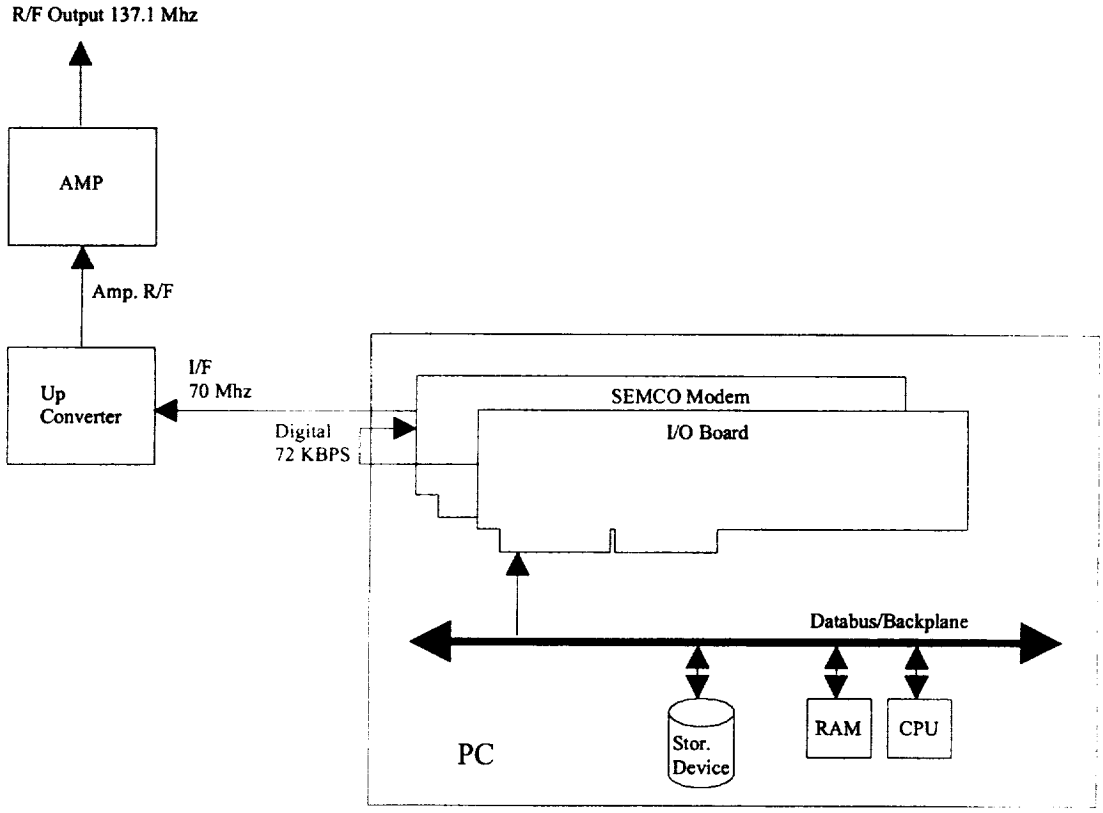

Figure 6. Transmitter Hardware Block Diagram

modulates the data to 70 MHz. The upconverter converts the signal to a 137.1 MHz R/F signal to be amplified and broadcast via an antenna. The baseband data rate is 72 KBPS.

2.1.1 SEMCO Modulation

The SEMCO MODEM was optimized for 72 Kbps at the factory. Therefore for this test program, to obtain the maximum efficiency, the data rate going into the modulator was restricted to 72 Kbps (72 Ksps I channel and 72 Ksps Q channel). Since the interleaver adds 8 synchronization bits (symbols), called a unique word (UW), for every 72 symbols,

this mandated reducing the information data rate to accommodate this overhead. Since the data rate expansion is 80/72, the result is 64.8 Kbps (64.8x80/72=72) prior to convolutional encoding plus 7.2 Kbps for the Unique Word. The SEMCO MODEM provides I and Q data paths into the QPSK modulator producing a 70 MHz QPSK IF signal at a 0 dBm level.

The Modulator provides a 72KHz Clock signal to synchronize the I and Q data streams from the I/O board. The data is expected to be valid on the rising edge of this Clock signal. The MODEM is based on the L3 COM PA100 digital spread spectrum receiver chip. It contains many features that are not used for the LRPT system.

2.1.2 I/O board

The I/O board is a modified version of the AVTEC's AT_HSIO2. It is a synchronous serial I/O board with 4k bytes of FIFO memory. A modification was performed to convert this board into a dual channel data I/O board providing parallel data to the I and Q inputs of the QPSK modulator.

The software driver is designed in multi-threaded structure so that the I/O process is running concurrently with other processing modules in the host.

2.2 Transmitter Software Description

The simulation software is a combination of several entities. AVHRR image data files are MLT compressed into stripes of 8 lines. The compressed files are then encapsulated into CCSDS packets by the packetizer program. This program inserts the appropriate application ID and calculates packet length. The resultant file is then inputted to the M_PDU generator. This program takes packetized compressed images and multiplexes them along with packets from non-compressed simulated sources. Refer to section 1.2.1 for a list of possible METOP source entities. For this system, all sources or APIDs are simulated and are scheduled according to the METOP data rates for each source. After M_PDUs are generated, VCDU headers are added along with R-S codes thus forming CADUs. The CADUs are then convolutionally encoded, interleaved and the UW is inserted. The resulting data is queued into the xmit-buffer awaiting transmission. A data driver takes the data and drives into the I/O card, which then directs the data into the SEMCO MODEM for QPSK Modulation and subsequent RF transmission.

2.2.1 Data compression

The Modulated Lapped Transform (MLT) is a NASA/GSFC Code 564 lossy data compression algorithm. Its coder consists of several functional modules depicted in Figure 7. The scan converter takes input imaging data and formats it into eight-by-eight blocks of integer values as input to the de-correlator. The de-correlator employs a hybrid transform that performs a size-8 MLT with sixteen input data points in the scan direction of imaging data, and a size-8 Discrete Cosine Transform (DCT) in the other direction. This hybrid transform, termed enhanced DCT (EDCT), uses overlapping blocks in the

scan line direction to reduce the blocking effect inherent in a two-dimensional (2D) DCT, but it allows isolation of strips of eight lines, as is often required by practical implementation in a packet data system. However, the system also allows an eight-by-eight 2D DCT, an eight-by-eight 2D MLT, or other types of block transform to be implemented.

The bit plane encoder (BPE) first groups the eight-by-eight transform domain components into three family trees; each has one parent, four children, and sixteen grandchildren. The magnitudes of components are scanned for any most significant bit (MSB) on the scanned bit plane. This bit-plane scanning proceeds from the top-most bit plane downward. The positional information of those identified components is represented by a family tree structure and may be further coded for efficiency. This information, along with associated sign information, is shifted to the output bit string from higher bit planes to lower bit planes.

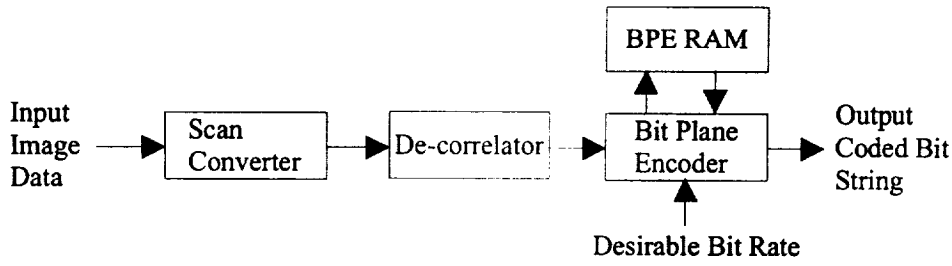

Figure 7. Functional Diagram of the Coder

The BPE random access memory (RAM) holds BPE-processed information for as many input blocks as it can support. The number of input blocks supported by this RAM is identified as one segment of input data. A segment can be as simple as one strip of eight lines, multiples of eight-line strips, or even half a strip. For purposes of LRPT, one strip of eight lines is the same as a stripe of eight lines.

The output bit string constitutes an embedded data format that allows progressive transmission and decoding to start at a lower bits per pixel (BPP) rate and proceed to a higher BPP rate. The bit string can be terminated at a desirable rate for precise control of output data rate. METOP defines a 10-to-1 compression ratio.

2.2.2 Data Simulator

After the stripes are compressed, a packetizer routine takes each stripe and places it into a single source packet. These source packets are then sent to CADU generator. This is a software program that produces CCSDS CADUs from files formatted in CCSDS source packets. It takes any packet files and puts them into the VCDU data unit zone according to channel number. Multiplexing order is accomplished by a scheduling scheme

according to the METOP specification. The resulting file is then convolutionally encoded, convolutionally interleaved and UW inserted. After processing the file resides in the transmitter hard-drive to await transmission.

2.2.3 Data Driver

This software routine takes the processed CADU file and delivers it to the hardware. It also tracks the number of CADUs that were transmitted.

Section 3: Ground Station System Description

A block diagram for the LRPT ground station/receiver is shown in Figure 8. The MODEM is a PC-based card produced by L3-Com and sold by SEMCO. After the antenna there is a Low-Noise Amplifier (LNA) that boosts the received signal. There is a down-converter before the front-end of the SEMCO board that takes the 137.1 MHz RF signal down to 70 MHz Intermediate Frequency (IF). The MODEM has a QPSK demodulator with tracking and bit-synchronizer functions. After the receiver has obtained lock and symbol synchronization, data is passed into an Input/Output (I/O) card in the PC's backplane where it is UW synchronized, de-interleaved, convolutionally decoded, CCSDS frame synchronized, CCSDS transition generator removed and R-S decoded. Data is then sorted by Virtual Channel number. MPDU Headers are processed and Packets are sorted by Packet ID. One complete packet represents one scan stripe. Each packet is passed on to the de-compressor and then to the screen for display. This system performs in real-time and as each stripe is received it is displayed before the next is received.

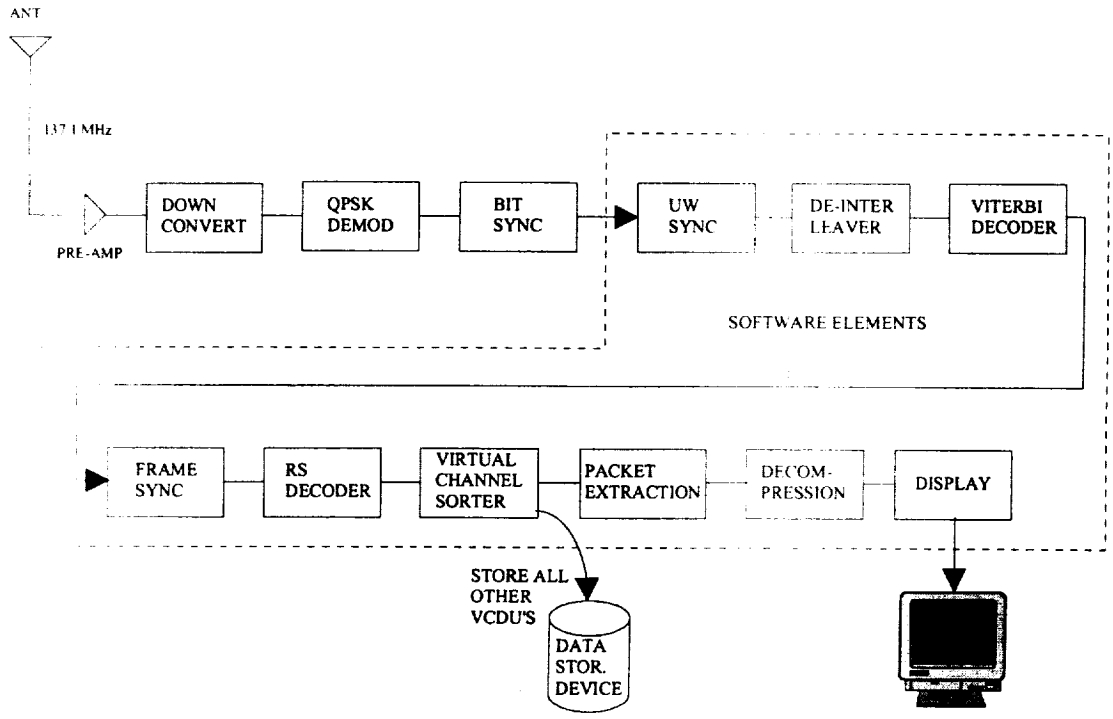

Figure 8. Receiver Block Diagram

3.1 Ground Station Hardware Description

The Ground Station comprises of a RF antenna, low noise pre-amplifier, down converter, receiver, and display. The RF signal is received through the antenna on the 137 MHz carrier. The down converter brings the RF signal to 70 MHz where the demodulator in

the SEMCO board produces soft-decision bits. These bits are then passed to the receiving software. Figure 9 is a block diagram of the Ground Station Hardware.

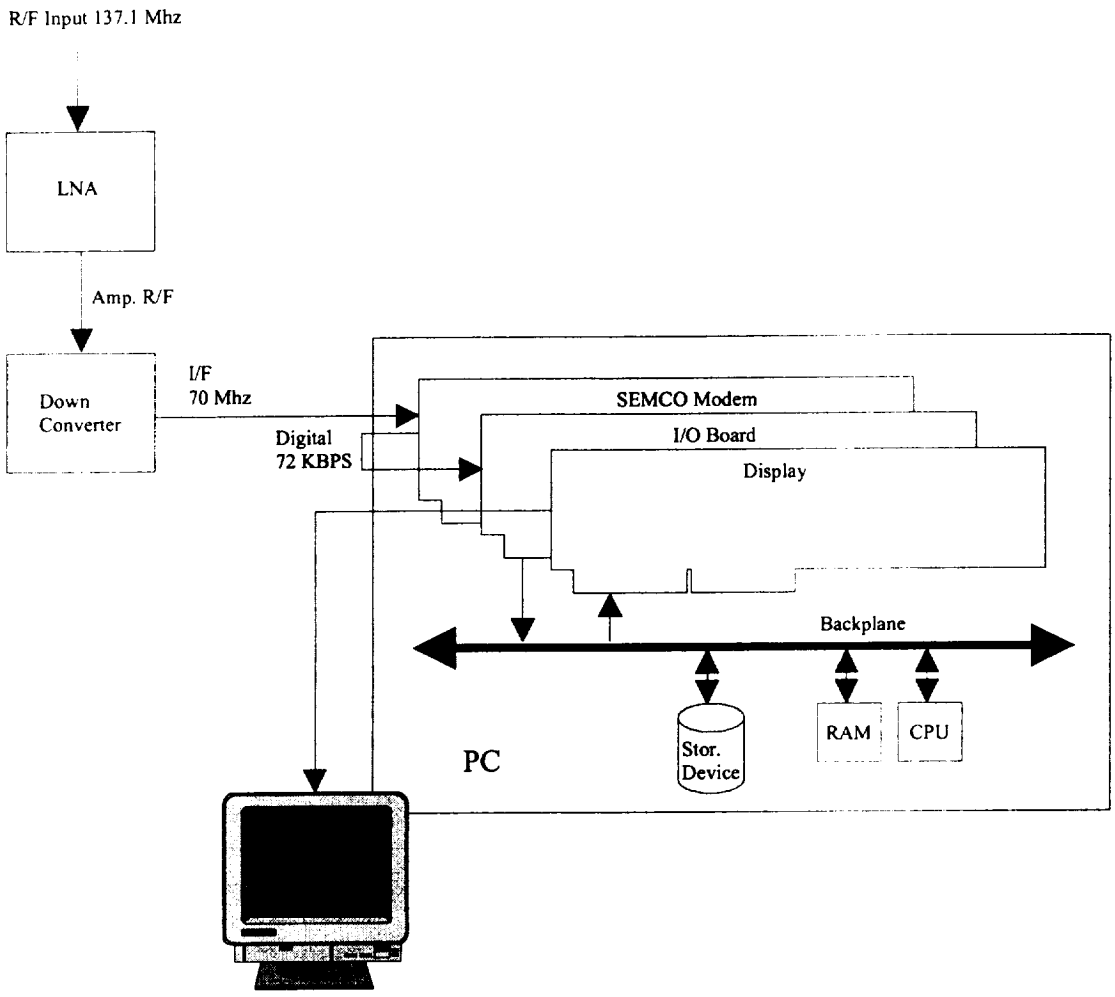

Figure 9. Receiver Hardware Block Diagram

3.1.1 SEMCO Demodulation

The SEMCO board performs QPSK demodulation, bit (symbol) synchronization and 3-bit soft-decision quantization. It provides 3-bit In-phase and Quadrature (I and Q) output data lines along with a received clock signal. An I/O board is used to read the 6 input lines (three I and three Q) in parallel and pack them into one byte. This byte is then read into the PC memory for software processing.

3.1.2 I/O board

The receiver circuit on the AVTEC AT-HSIO2 board was modified from a serial (single data stream) synchronous channel to six parallel channels. This is to accommodate the 3-bit I and 3-bit Q soft decision data from the QPSK Demodulator/Bit Sync. The I/O process is running in parallel with other processing modules (Frame Sync, De-Interleave, Viterbi) with a 4k bytes of FIFO as a buffer. This buffering allows the CPU to run in multi-tasking/multi-threaded mode without loss of data from the I/O board.

3.2 Ground Station Software Description

The software's main goal is to process the received soft decision data from memory and display it on the monitor. The original plan was to separate the software into two programs in order to run on two separate machines. However, the processing speeds in the new PCs are such that only one machine is needed to perform the necessary functions in real-time. Furthermore, only 40% of the CPU bandwidth of a Pentium II 400 MHz based PC was needed for the entire software processing.

The software can be described as a set of modules working in sequence. Sections 3.2.0, 3.2.1, 3.2.2 outline the Physical Layer routines while sections 3.2.3, 3.2.4, 3.2.5 describe the upper layer processing.

3.2.1 Unique Word Frame Synchronizer

Unique Word (UW) Frame synchronization is the first data processing software routine. Data is passed to the synchronizer in a 1280 byte buffer; each byte contains one I and one Q soft-decision word (3-soft decision bits each). A convolutional interleaved frame is 80 bits, 72 data bits for every 8 bits synchronization (UW). Therefore, each buffer contains 32 frames or 2560 total bits. The synchronizer's function is to identify the most likely location of the UW in the data buffer. It also resolves the phase ambiguity and lines up the data for the de-interleaver. Figure 10 shows a State Diagram of the synchronization routine.

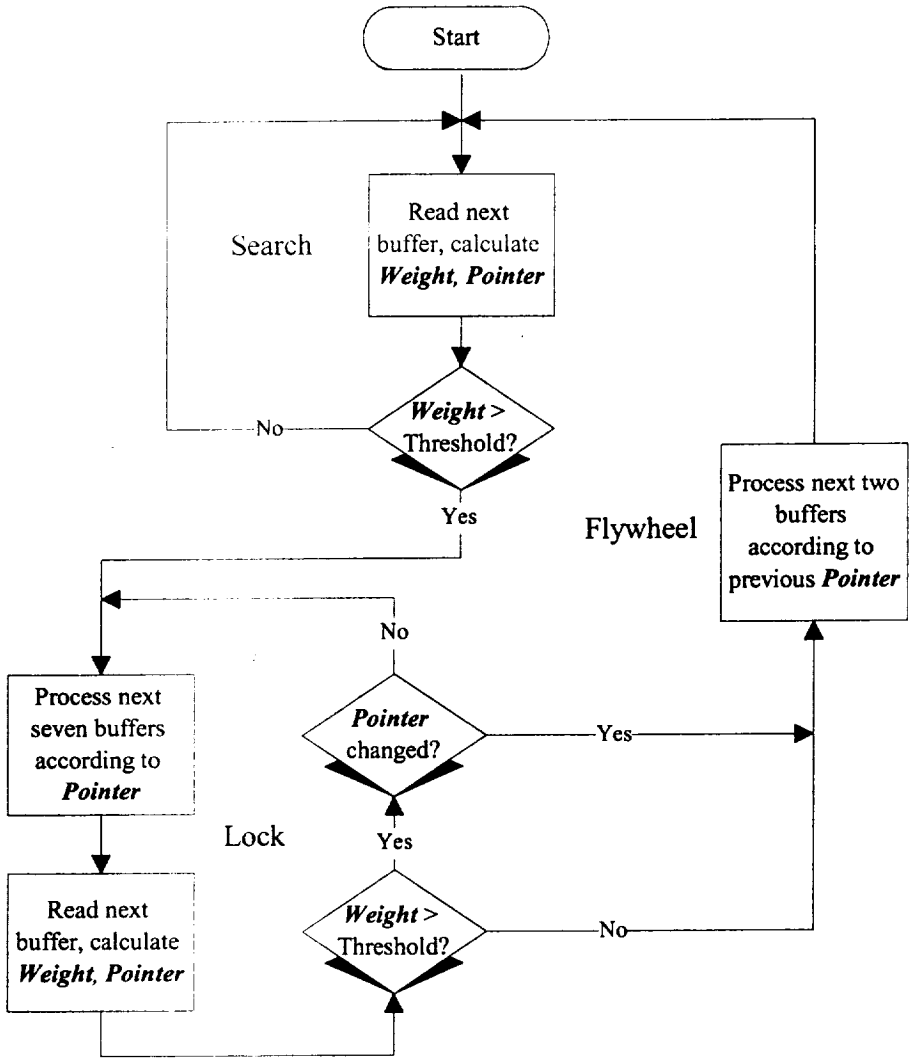

Figure 10. UW Synchronization Flow Diagram

Its operation can be described in three modes: Search, Lock and Flywheel. It starts out in Search mode. In this mode the UW byte is correlated, as defined in Equation 1, with

$$Weight_i = \sum_{j=0}^{31}\sum_{k=0}^{7} Buffer[i+80j+k] \oplus \overline{UW[k]} \qquad i = 0,1,2,....79$$

Equation 1. UW Correlation Function

every possible frame location in the data buffer. *Weight* is the correlation function, *Buffer*[] refers to the current data buffer, *UW*[] is the Unique Word and *i* is the bit index. Note that the UW is negated in the equation to mask or provide a proper weighting factor. This function will scan through the entire data buffer. The *i* with the maximum *Weight* or highest correlation, defined as "pointer", will point to the most likely start of the UW. Once identified, the entire buffer is shifted so that the first byte is the UW. Once the data is aligned, the buffer is passed on to the de-interleaver. If the maximum weight meets a minimum threshold then the synchronizer would be deemed in a Lock mode. If that threshold is not met, then the data is still processed according to the highest weight but the synchronizer would stay in Search mode for the next buffer. The synchronizer will only lock when the minimum threshold is achieved. Once in a Lock mode, the same pointer is used for the next six buffers after which the synchronizer will enter Search mode again to determine if the minimum threshold is still met and the pointer has not changed. If there is a discrepancy, the synchronizer will enter the Flywheel mode where the older pointer is used for two buffers. After which a Search is performed and if the discrepancy still exist then the new pointer is used to align the data. At which point the process enters the Lock mode again and the cycle repeats itself.

3.2.2 De-Interleaver

The de-Interleaver takes the UW synchronized data buffers and processes in software via address calculation. Data is serially written into memory but read out by incrementing the readout address for each branch and for the added memory delay, M, in each branch. After the de-interleaver uses the UW for synchronization it will be eliminated so that only the convolutional symbols are delivered to the decoder.

The de-interleaver scatters a burst error so that the Viterbi can perform the correction. This de-interleaver has 36 branches with memory delays of 2048 so that two adjacent bits are separated by 36 x 2048 = 72728 positions. This translates into an allowance for error burst time of about 1 second in the 72kbits/sec system. Refer to reference [5] for a more detailed explanation of this technique.

3.2.3 Viterbi Decoder

The Viterbi Decoder is responsible for the Maximum-Likelihood-Decoding of the Convolutional Code. Although computationally intensive, this decoder is the industry standard procedure for convolutional decoding.

The Viterbi Decoder software was adapted from a shareware package by Phil Karn of Qualcomm. It is optimized for a Pentium Computer and can decode at about 300kbits/sec

on a 300MHz Pentium computer. It uses the common Add-Compare-Select algorithm. Description of the Viterbi Algorithm can be found in a number of technical books [4-6]. The original code is written for 8-bit soft decision data so the 3-bit data soft decision data originating from the QPSK Demodulator/Bit Sync has to be extended (padded with zeros) before going into the Viterbi.

3.2.4 CCSDS Processor

This software routine provides Frame synchronization, R-S decoding, Virtual channel sorting and packet extraction. Frame synchronization is similar to the UW synchronization except the synchronization word is 32 bits long and the frame size is 8192 bits. This routine also provides statistical information relating to R-S decoding, i.e. number of correctable errors, lost frames, etc. Steve Duran of JSC provided this software originally intended for use in a UNIX platform.

Further information on the necessary processing functions can be found in the publications of CCSDS on Advanced Orbiting System [2].

3.2.5 MLT Decompressor

The Decompressor performs the exact same functions as the compressor described in section 2.2.0 except it works in reverse order. It takes each compressed stripe and outputs eight scan lines.

3.2.6 Display Driver

The purpose of the driver is to take the data from the MLT Decompressor, sub-sample the data and display on the monitor. Since the image is transmitted in strips (8 lines x 2048 pixels), a 4-to-1 sub-sampling producing an 8 x 512 image is displayed on the screen in gray scale. Strips are continually panned upward in a manner similar to how a push broom sensor is capturing the image. Once an entire screen buffer is filled, the entire image is panned with the latest strips displayed on the bottom.

Another function of the Display Driver is to show up-to-date real-time status of the software modules, i.e. synchronizer, CCSDS processor; and also accumulate statistics, e.g. Bit Error Rate, lost frames, etc.

Section 4: Environment Simulator

The environment simulator is composed of two parts, a Scintillation generator and a Man-made noise/Gaussian noise generator. Both the Man-made/Gaussian noise generator and the Scintillation generator are based on studies performed by the Institute for Telecommunications Sciences (ITS) [3,7].

The ITS Man-made noise study consists of collected noise data from several chosen sites: urban, suburban, and rural areas [3]. This data was analyzed and modeled into a program that generates noise signal patterns. These patterns form the basis of the noise generator.

ITS researched and analyzed Scintillation or fading effects at this band. This led to a separate model for this phenomenon [7]. A program was developed to generate noise data patterns based on the model and a Scintillation generator was built using the data patterns.

4.1 Noise Environment

The ITS study measured the noise levels at the 137 MHz band at several locations in Colorado [1]. These sites are categorized into business, residential and automotive locations. From the ITS study two data sets were selected and analyzed: Downtown Denver II and Lakewood I. Downtown Denver was selected because it represented a high noise urban area and Lakewood I was picked for its residential lower noise environment. These sites constitute the main focus of this study.

4.1.1 Man-made noise

Man-made noise is produced by sources such as automobiles, electrical distribution networks, and electronic devices. This noise is generally impulsive in nature and Poisson distributed.

4.1.2 Gaussian noise

Gaussian noise is the result of black body radiation (thermal noise), such as found in resistors. When this type of noise is characterized by a Gaussian amplitude distribution with an essentially uniform power distribution around the bandwidth of interest, it is known as White Gaussian noise. This study assumes that the Gaussian noise is White Gaussian noise.

4.2 Scintillation

When the Sun's rays strike air molecules in the Ionosphere, a plasma of free electrons and positively charge ions is produced. The free electrons will interact with the Space to Earth RF Communications at the 137 MHz band causing irregularities in the RF signal. These irregularities vary over time producing "Scintillation" effects on the received signal. The behavior of which can attenuate the signal and produce phase shifts in slow

fadeouts. Mathematically, this can be modeled by a Raleigh distribution. ITS has produced software that can generate Scintillation vectors that will be used to simulate this behavior.

4.3 Environment Simulator Architecture

From the noise model, amplitude and phase of the Man-made/Gaussian noise is converted into data files. These files are then loaded into a high-speed pattern generator that outputs the patterns every 5 microseconds (200 KHz). Two channels, one for amplitude and the other phase, drive a digital attenuator and a digital phase shifter respectively, modulating a 137 MHz sinusoid supplied by a signal generator. The noise controller (Personal Computer) controls the start and stop of the Man-made/Gaussian noise generator and loads the noise simulator with the data patterns.

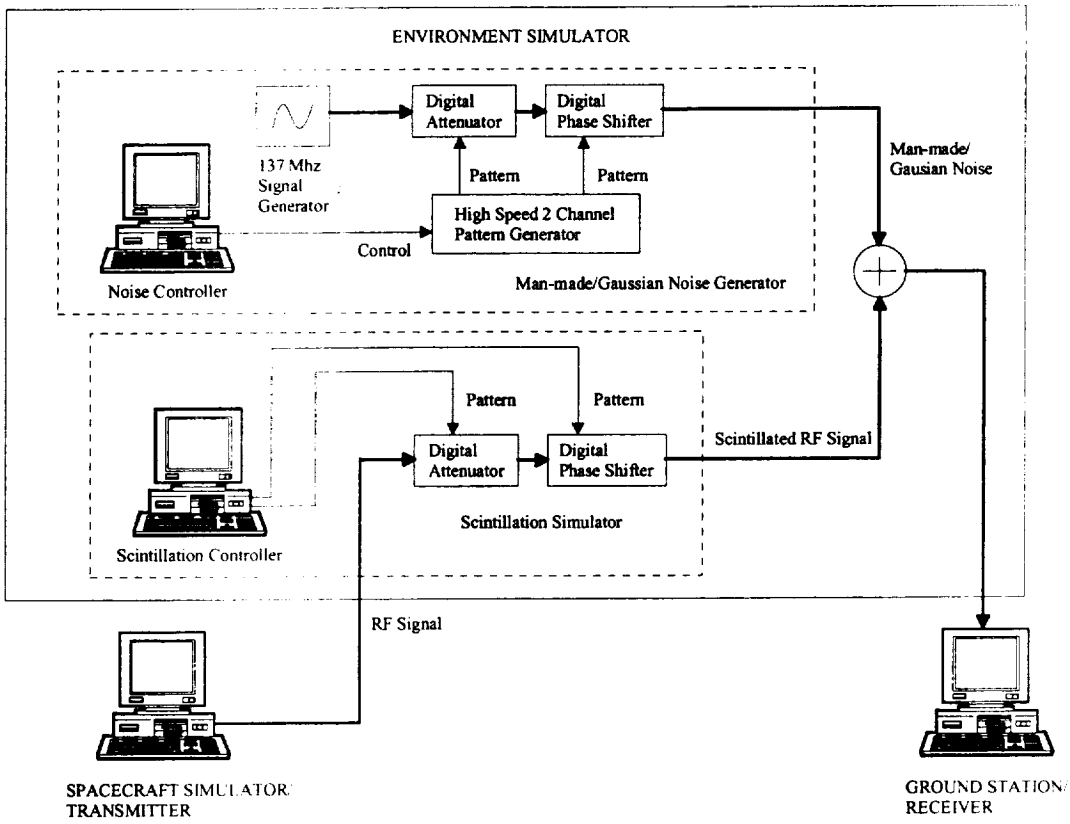

Figure 11. Environment Testing Configuration

The Scintillation generator is architecturally similar to the noise generator except that a pattern generator card is installed in the Scintillation controller itself. The ITS Scintillation model is reformatted to drive a digital attenuator and a digital phase shifter much in the same manner as the noise simulator. However, in this case, the source for the simulator is the RF signal from the transmitter and the patterns are updated at a 10 Hz rate. The total Environment Generator is the sum of both the Man-made/Gaussian noise

and the Scintillated RF signal. Figure 11 shows a block diagram of the complete environment simulation configuration.

4.4 Environment Patterns

Table 1 shows the profile of each of the two data sets. For more details on the characteristics of these environment profiles refer to the ITS Man-made noise report [3]. The total noise power figure is derived from output of the ITS noise model. This model of the noise was produced in a Fortran program whose output format is of a standard ASCII text file. This file consists of real and imaginary components of noise generated at 5 microsecond increments (200 KHz). A program was written to convert the real and imaginary parts into amplitude and phase. Further processing was needed to format the data into a file the pattern generator would accept.

Location	Noise Environment or Source	Total Noise Power (dBm)
Downtown Denver II	Business	-102.1
Lakewood I	Residential	-114.4

Table 1. Environment Profiles

The same is generally true for the Scintillation model. ITS analyzed the atmospheric Scintillation in a Link Analysis document. A program was written to produce patterns used to attenuate and phase shift the RF transmitted signal in a manner similar to the noise generator. The same type of reformatting is needed to convert the patterns for the Scintillation pattern generator internal to the controller. The program provided by ITS requires a Scintillation index as input [7]. For all Scintillation tests, the Scintillation index is 0.45.

Section 5: Environment Testing

The first phase of testing consists of three test configurations: 1. Man-made and Gaussian Noise, 2. Scintillation and Gaussian Noise, and 3. Man-made, Scintillation and Gaussian noise. Each combination represents a possible environment scenario. The major goal of the testing is to determine the performance of the protocol particularly the channel coding and how this translates to the performance of a ground station in the two data sets. Also most of the testing is summarized by the use of Bit-Error-Rate (BER) performance curves, which provide a convenient mechanism for comparisons. A detailed equipment and test procedures description is documented in a separate report [8].

The second testing phase consists of constructing a satellite path simulation using link analysis [7, 8] along with environment profiles in Table 1. The measurements were compared to two types of ground antennas (Omni and Yagi) along with three different satellite path elevation angles (30, 60 and 87 degrees). From this data, it can be determined how different receiving equipment will perform in different noise environments from the standpoint of a ground station tracking a satellite pass.

5.1 Man-made and Gaussian Noise Test

This test involves first mapping the receiver performance in the presence of Gaussian Noise only. With a Pseudo-Random Number (PN) generator as the data source and the use of UW synchronization at the channel symbol level, the channel BER performance of this step is used as a baseline when comparing with other performance curves. Also this can be used to determine the implementation loss of the receiver. Note that the data is collected at the output of the UW synchronizer on the receiver (refer to Figure 8). Once this is completed, Man-made and Gaussian noise is generated and the performance is mapped at the output of the Viterbi decoder. As a result, the effect of Man-made noise can be measured and isolated when comparing the Man-noise/Gaussian noise curve with the Gaussian noise only curve. Note that the environment profile is that of the Lakewood I site.

5.2 Scintillation and Gaussian Noise Test

This test provides testing data for a ground station with Scintillation and Gaussian noise. The data source is again a PN generated file that has UW synchronization. This test provides information as to how much of a contribution Scintillation has on the receiver performance. In other words, this test can isolate just the Scintillation effect on the BER performance of the receiver.

5.3 Man-made/Gaussian noise and Scintillation Test

This test combines the effects of both Man-made/Gaussian noise and Scintillation. The BER performance is mapped and compared with the Gaussian only case. Another goal of this test was to determine the efficacy of the interleaver. The interleaver was removed from the protocol and BER performance was again measured. This was compared to the

case with the interleaver. This comparison is performed at the output of the Viterbi decoder.

5.4 Satellite Path Simulation Test

This test uses the Man-made/Gaussian noise and Scintillation profiles of Section 5.3. It goes one step further by having a satellite pass simulated through the use of programmable attenuator from the Scintillation simulator. The link calculation is added with the Scintillation effect along every point of the pass. Also included are the antenna patterns of the satellite and receiver. Instead of a PN file, AVHRR images are formatted and used as the data source for this test. A table is generated detailing when and where data is acquired. Performance comparisons based upon elevation angles, receiver antennas and environment profiles are drawn. The test configuration is the same as shown in Figure 11.

Section 6: Bit Error Rate Results

The Man-Made simulations for Sections 6.1 and 6.3 are based on the Lakewood Noise profile. However, Section 6.3 also includes the Downtown Denver profile testing, which of the two profiles is the noisiest case. The test data from Sections 6.1 and 6.3 are from the output of the Viterbi decoder. Attempts were made to obtain data from the output of the Reed-Solomon decoder (or fully coded) for the Lakewood profile with Scintillation. The fully coded test has such a high coding gain that the channel bits start with a high error rate. Hence, making measurements at the channel error rate when fully coded is difficult. However, it was noted that after achieving lock the fully coded receiver/protocol operated with virtually error-free as long as the receiver maintained solid lock [8].

6.1 Man-made and Gaussian Noise Results

The Bit-Error-Rate results of this test are shown in Figure 12. The curves demonstrate the performance of the interleaver and convolutional coding. Referring to Figure 8, the Viterbi decoding takes place after the UW synchronization and de-interleaver. It is at this point that the protocol differs from the CCSDS recommendations and is specific to EUMETSAT specification. Note that at 10^{-5} BER, there is a 7.5 dB E_b/N_0 difference between the Man-made noise curve and the Viterbi output curve (this can be seen by noting that at 10^{-5} BER, the Viterbi curve is at 10.5 dB and the Man-Made/Gaussian curve is 18 dB). Therefore the combination of interleaving and convolutional together provides a 7.5 dB gain in the presence of Man-made and Gaussian noise at 10^{-5} BER. At 10^{-4} BER there is a 7 dB gain. This noise was generated by the ITS for a Residential profile specifically Lakewood I. It is worthy to note that at higher BER i.e. around 10^{-3} (where the system will operate in order to take advantage of the R-S coding) the gain is 5.2 dB. Therefore the Viterbi output demonstrates a 5.2 dB coding gain in the presence of Man-made noise. These results confirm that the interleaving along with convolutional code provides good performance in this environment.

Note that there no data points from the Viterbi above 3 $x10^{-3}$; the receiver could not attain bit synchronization at this region. This is due to the quality of the receiver. Referring to Figure 12, the bit synchronizer portion of the receiver looses lock at 2.5 dB in the presence of Gaussian Noise and about 3.4 dB for Man-Made/Gaussian Noise. It can also be determined that the coding gain at 3 $x10^{-3}$ BER is about 3.9 dB. This explains why the receiver can no longer synchronize above 3 $x10^{-3}$ BER because it is at this point where the Viterbi is operating at 7.7 dB and the bit sync is actually working at approximately 3.8 dB. This is around the condition where the receiver under Man-Made/Gaussian Noise looses bit synchronization (see Man-Made/Gaussian Noise Curve of Figure 12). At the Viterbi output curve, the region above the data point at 2 $x10^{-4}$ BER appears to show degradation in the receiver performance as the curve appears to move vertically (larger negative slope) and therefore no longer tracks the performance of the Gaussian Noise or the Man-Made/Gaussian Noise curve.

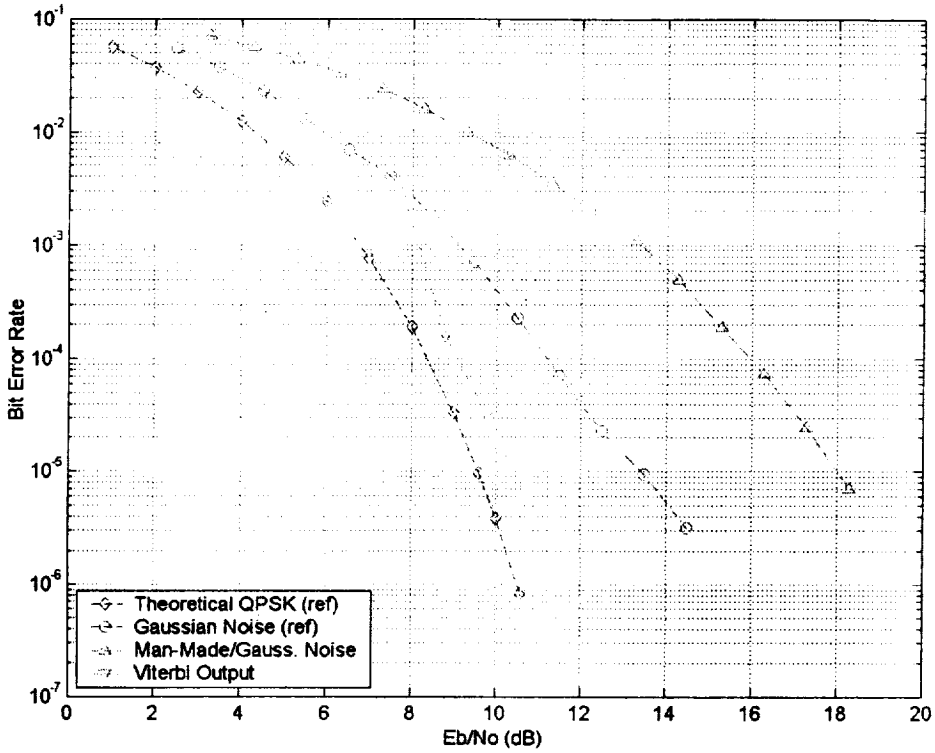

Figure 12. Man-Made/Gaussian Noise (Lakewood I)

When comparing the Gaussian noise curve with the Man-Made/Gaussian noise curve, there is as much as 5 dB difference at 10^{-4} BER. Therefore Man-Made noise can be said to cause as much as 5 dB additional loss in the receiver system.

Also, as can be observed by comparing the theoretical QPSK BER curve with the Gaussian Noise curve that there is as much as 4.5 dB implementation loss at the front end of the receiver. This is typical of a receiver of this quality.

6.2 Scintillation and Gaussian Noise Results

This test was devised in order to determine the impact of the Scintillation phenomena on the BER performance. The results of this test are summarized in Figure 13. The comparison of the two curves demonstrates a fairly uniform difference of 1.75 dB between the Gaussian Noise curve and the Gaussian Noise with Scintillation curve. In other words, Scintillation contributes to a 1.75 dB loss of performance in addition to Gaussian Noise.

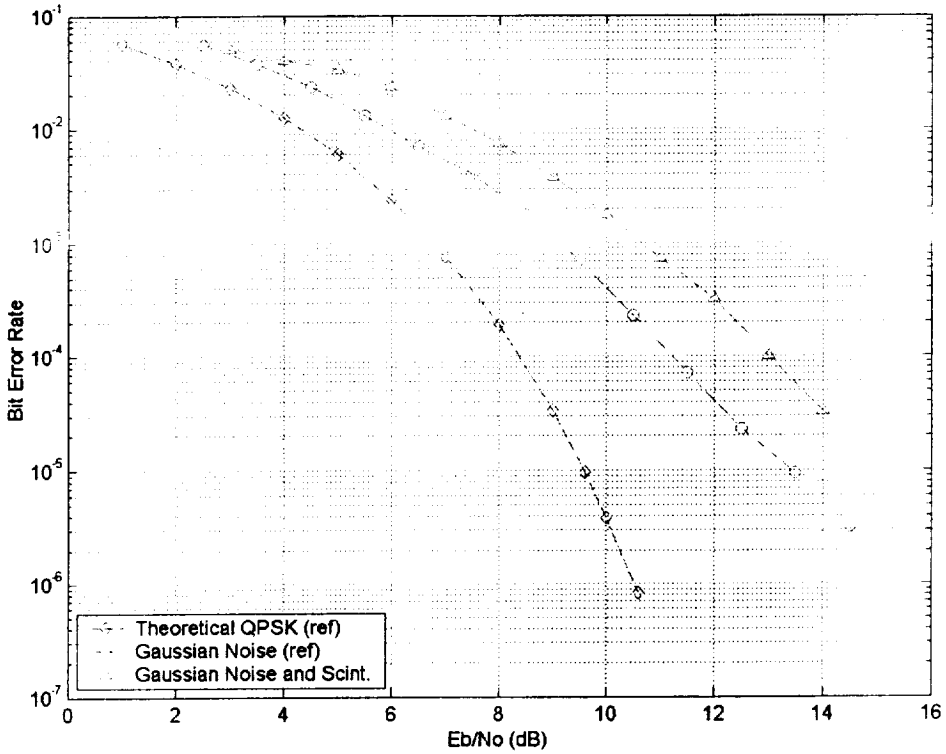

Figure 13. Gaussian Noise and Scintillation Test

6.3 Scintillation with Man-Made and Gaussian Noise Results

From Figure 14, for Lakewood I, the Man-Made/Gaussian with Scintillation curve differs from the Gaussian Noise around 5 dB at 10^{-4} BER. Therefore Man-made Noise with Scintillation contributes to a 5 dB loss at 10^{-4} BER. Compare the Man-Made/Gaussian with Scintillation of Figure 14 and the Man-made/Gaussian Noise curve without Scintillation in Figure 12. There is a 0.25 dB difference at 10^{-4} BER. This means that in the presence of Man-made noise, the Man-made impulsive noise overwhelms the slow fading Scintillation effects. To confirm this, note that without Man-made noise, section 6.2 demonstrates a larger 1.75 dB difference. This conclusion is viewed from the output of the Bit-Synchronizer/UW Synchronizer.

From the viewpoint of the Viterbi decoder, the Man-made/Gaussian Noise with Scintillation and interleaving has a 7 dB gain at 10^{-4} BER with a value of 9.1 dB. From Figure 12, the Man-made/Gaussian Noise at the Viterbi decoder has a 7 dB gain at 10^{-4} BER with a value of 9.1 dB. Therefore, the code gain is the same with or without Scintillation. Moreover, there is 2 dB difference between the values. This is approximately consistent with the 1.75 loss from section 6.2 and would imply that the interleaver does provide sufficient spreading of the burst errors to be effective. And, if we remove the interleaver, Figure 14 shows a 1.7 dB (at 10^{-4} BER) difference between the receiver with and without the interleaver. The largest difference between the two

curves is about 2 dB at 10^{-3} BER. The curves would imply that as the BER reduces below 10^{-5}, the two curves of Viterbi outputs, with and without interleave, appear to converge. This is what would be expected due to the fact that as the errors get more infrequent, the effect of the interleaver diminishes. On the other hand, when operating at about 10^{-3} BER with R-S decoding the interleaver will be valuable, as expected.

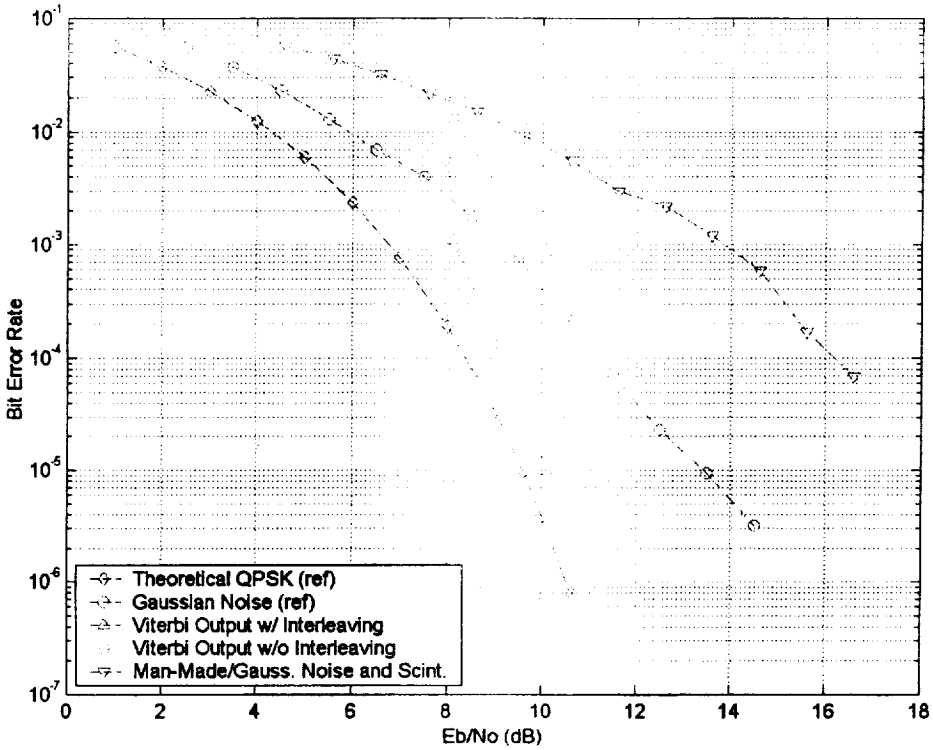

Figure 14. Man-Made/Gaussian Noise and Scintillation Test (Lakewood I)

Referring to Figure 15, the same testing was performed on the Downtown Denver II profile. This is a noisier Man-made environment in terms of noise power and increased impulsive noise. At 10^{-4} BER, there is a 16.6 dB requirement at the receiver system versus the 16.2 dB for the Lakewood II case. The Viterbi with interleaver performance at 10^{-4} BER is about a 5.2 dB gain versus 7dB gain for Lakewood II. And there is a 1.3 dB difference at 10^{-4} BER between the Viterbi with and without interleaving as compared to the 1.7 dB with Lakewood II. The Viterbi curves at around 10^{-2} BER and above exhibit the same degradation as the Lakewood II case. As in both cases the degradation is most apparent around the 8 dB on the Viterbi output curves where synchronization begin to fail. From Figure 15, the Viterbi with and without interleaver, above 10^{-2} BER, show an actual coding loss. This is not surprising given that noise is not only Gaussian but has Man-made noise components and the BER is very high.

In the Lakewood testing, the convergence of the Viterbi curves seems apparent, however in the Denver case, the convergence is not apparent. It can be reasoned that with increased impulsive noise, convergence may occur at a lower BER.

It can be concluded from this data that code gain is affected by the statistical noise of the environment. As expected, those environments with more Man-made noise can actually reduce the coding gain. In residential type areas, the interleaver performs as designed and helps mitigate fading and burst noise.

As mentioned earlier, characterizing the receiver at the output of the R-S decoder (or fully coded) presented difficulties. Due to the very high coding gain, a large negative slope is expected for the BER curve. As a result, the sensitivity of BER performance to small changes in E_b/N_0 is large. This therefore limited the ability to obtain enough data points to graph the BER curve. It was observed that the receiver's front-end required a minimum of 4.5 dB Signal-to-Noise Ratio to maintain solid lock. This translates to about 8.7 dB E_b/N_0 at the R-S decoder output. Efforts to obtain enough data points to graph the BER curve beyond this threshold were not successful.

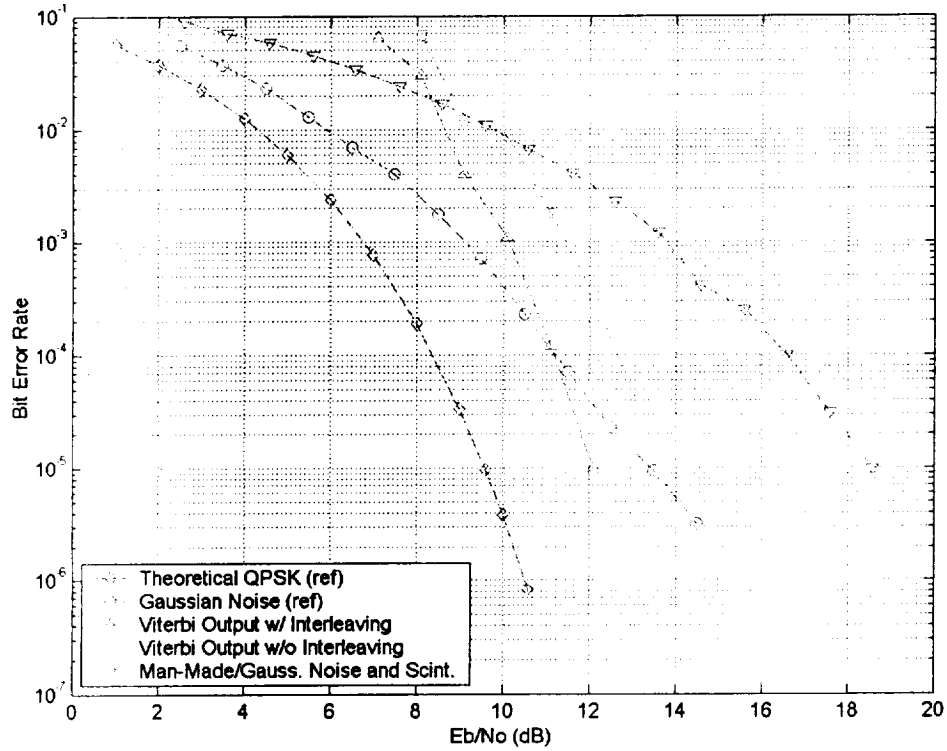

Figure 15. Man-Made/Gaussian Noise and Scintillation Test (Downtown Denver II)

Section 7: Satellite Path Simulation

This phase of the testing consists of taking the METOP specification for satellite power and antenna gain; performing link analysis [8] and simulating a satellite path for three different maximum elevation angles—30 degrees, 60 degrees, and 87 degrees. Also included are the two environments Lakewood II and Downtown Denver I, along with two types of receiving antennas: Omni-directional and Yagi with satellite tracking. The results are summarized in Tables 2-5. Lock is achieved when data first appears on the monitor and lost when the last data line finishes. Range is the distance to the simulated spacecraft from the ground station antenna. Elevation Angle is the angle above horizontal from the ground station antenna to the simulated spacecraft. A time of zero is defined to be the beginning or at the horizon of the path simulation and runs until the path finished. Note that threshold of acquisition is higher than that point which the receiver loses lock. This is a common quality with all receivers. The main column that summarizes this test is the Acquisition Time as percentage of the total pass time. This figure will show the percentage of data that can be collected out of the total available given the environment and antenna type.

7.1 Downtown Denver II Results

Tables 2 and 3 summarize the testing for this environment. Table 2 demonstrates that even with an Omni-directional antenna, useful data acquisition can occur even on passes with the maximum elevation as low as 30°. Acquisition occurs 181 seconds after the satellite comes over the horizon. Therefore some of the data cannot be received due the low E_b/N_0. In fact 65% of the path data can be acquired leaving 35% of the data lost. The performances for the 60° and 87° maximum elevation path simulations are similar as the table shows. However in these cases the acquisition times are about 5% greater as somewhat expected.

When a high gain tracking Yagi antenna is used, acquisition times can be greatly improved as shown in Table 3. The effect of using a Yagi, which has an 8 dB higher gain than the Omni, has a net improvement of 6.8 dB on the link. This is enough to provide close to 100% acquisition times during satellite view times, resulting in close to zero available data losses.

The METOP spacecraft antenna is designed to give a 5 dB higher gain in the direction of the horizon as compared to nadir. This results in a greater Equivalent Isotropic Radiated Power (EIRP) on the horizon where the receiving ground station is at a greater range than one directly below. This affects the range figures in Table 2, as the range at Lock Acquired and Lock Lost of the 30° maximum elevation is greater than that of the 87° maximum elevation.

Path Type	Sync. Status	E_b/N_0 (dB)	Range (km)	Elevation Angle (deg)	Time (sec)	Acquisition Time (Percentage of Total Path Time)	Max. E_b/N_0 (dB)
30° Max Elevation	Lock Acquired	3.8	2248	12.5	181	65%	6.9
	Lock Lost	2.6	2583	7.8	720		
60° Max Elevation	Lock Acquired	4.0	2207	13.1	170	70%	7.7
	Lock Lost	2.6	2576	7.9	794		
87° Max Elevation	Lock Acquired	4.1	2186	13.4	169	69%	7.7
	Lock Lost	2.9	2496	8.9	790		

Table 2. Downtown Denver II with Omni-directional Antenna

Path Type	Sync. Status	E_b/N_0 (dB)	Range (km)	Elevation Angle (deg)	Time (sec)	Acquisition Time (Percentage of Total Path Time)	Max. E_b/N_0 (dB)
30° Max Elevation	Lock Acquired	7.5	3132	2.1	28	97%	13.5
	Lock Lost	7.1	3239	0.9	830		
60° Max Elevation	Lock Acquired	7.5	3122	2.2	28	97%	14.3
	Lock Lost	7.2	3222	1.0	893		
87° Max Elevation	Lock Acquired	7.7	3110	2.3	40	96%	14.5
	Lock Lost	7.4	3226	1.0	900		

Table 3. Downtown Denver II with High Gain Yagi Tracking Antenna

7.2 Lakewood I Results

For the Lakewood environment, results in Tables 4 and 5 show that regardless of the two types of antennas studied, acquisition times are very close to 100%. This is due to the fact that the quieter environment (as opposed to Downtown Denver) will result in less interference loss. When comparing the Maximum E_b/N_0 figure of the Lakewood to Downtown Denver results (Tables 2 to Table 4), there is as much as 13 dB margin rendering the choice of antennas insignificant.

Path Type	Sync. Status	E_b/N_0 (dB)	Range (km)	Elevation Angle (deg)	Time (sec)	Acquisition Time (Percentage of Total Path Time)	Max. E_b/N_0 (dB)
30° Max Elevation	Lock Acquired	12.9	3212	1.3	15	98%	19.2
	Lock Lost	12.8	3239	0.9	830		
60° Max Elevation	Lock Acquired	13.2	3127	2.2	28	97%	20.0
	Lock Lost	12.9	3222	1.0	893		
87° Max Elevation	Lock Acquired	13.0	3203	1.4	29	97%	20.0
	Lock Lost	12.9	3226	1.0	900		

Table 4. Lakewood I with Omni-directional Antenna

Path Type	Sync. Status	E_b/N_0 (dB)	Range (km)	Elevation Angle (deg)	Time (sec)	Acquisition Time (Percentage of Total Path Time)	Max. E_b/N_0 (dB)
30° Max Elevation	Lock Acquired	19.8	3132	2.1	28	97%	25.8
	Lock Lost	19.4	3239	0.9	830		
60° Max Elevation	Lock Acquired	19.8	3122	2.2	28	97%	26.6
	Lock Lost	19.5	3222	1.0	893		
87° Max Elevation	Lock Acquired	19.8	3203	1.4	29	97%	26.8
	Lock Lost	19.7	3226	1.0	900		

Table 5. Lakewood I with High Gain Yagi Tracking Antenna

Section 8: Conclusion

The goal of producing a low-cost METOP LRPT compliant receiver using COTS equipment was realized with good results. Not only was this goal achieved, but it was also demonstrated that a majority of the receiver front-end could be synthesized in software. And this software, when running on a 400 MHz Pentium II based PC, can maintain real-time performance while expending only 40% of the CPU bandwidth. As a result, placing most of the front-end processing in software will considerably reduce the cost of the RF MODEM and will lead to very inexpensive ground stations.

The primary goal of Phase II is the performance testing of the LRPT protocol in an RF environment. The design and development of an environment simulator provided a means for protocol performance testing as well as the simulation of a satellite pass at different maximum elevation angles.

The BER results show 7 dB of coding gain at the output of the Viterbi decoder at 10^{-4} BER in a residential environment with Man-made/Gaussian noise and Scintillation. This coding gain was found to decrease to 5.2 dB as the Man-made noise increased for the urban environment. Also, it was found that the performance at the output of the R-S decoder was virtually error-free as long as the receiver maintained solid lock. In the case of the SEMCO receiver this was at a minimum Signal-to-Noise Ratio of about 4.5 dB. Although this inexpensive receiver was sufficient for this experiment, it does not work at a low enough E_b/N_0 to take advantage of the high coding level required to provide near 100% coverage by a METOP system in a high noise environment.

The pass simulations prove that data acquisition is possible in residential environments such as Lakewood, Colorado could achieve nearly 100% of the total acquisition time regardless of whether a Yagi or Omni antenna was used. Whereas high noise urban environments such as Downtown Denver, Colorado 65% of the total acquisition time can be achieved even with an Omni antenna. However in larger more populated metropolitan areas, it may be advisable to use a tracking Yagi antenna due to the noisier environments.

In conclusion, given the type and quality of equipment used, it is evident from the simulation results that the METOP protocol performs to the environments it was designed for. And the channel coding provides proper coding gain for Man-made/Gaussian noise while at the same time the interleaver mitigates the Scintillation phenomena. While the current COTS compatible MODEMs are not specifically designed for LRPT and thus are not fully optimized for the protocol, future compliant MODEMs should demonstrate better performance than the equipment used for this study.

Section 9: Demonstration

The demonstration utilizes the configuration outlined in Figure 11. Three images of different wavelengths of AVHRR data from the Southern India region were consecutively sent. These images are transmitted continuously to demonstrate the real-time capability of the receiver. A satellite pass simulation is performed with one of the two environments selected for simulation. The receiver's monitor displays the decoded transmitted image along with statistical information about the synchronization and channel decoding. Observers can monitor when a satellite pass is close enough to acquire data and when it's far enough to loose data.

References

[1] HRPT/LRPT Direct Broadcast Services Specification, EPS/METOP Programme, ESA/EUMETSAT, Doc. No. EPS/SYS/SPE/95413 and MO-DS-ESA-SY0048, Issue/Rev: 5, Feb. 1, 1998.

[2] Consultative Committee for Space Data Systems, CCSDS, Advanced Orbiting Systems, Networks and Data Links: Architectural Specification, Blue Book, CCSDS 701.0-B-1, October 1989.

[3] Man-made Noise at 137 MHz, R. Achatz, Y. Lo, P. Papazian, R. Dalke, G. Hufford, National Telecommunications and Information Administration, Institute for Telecommunications Sciences, interagency document.

[4] Principles of Digital Communication and Coding, Andrew Viterbi and Jim Omura, McGraw Hill, 1979.

[5] Error Control Coding: Fundamentals and Applications, Shu Lin and Daniel Costello, Prentice- Hall, 1983.

[6] Digital Modulation and Coding, Stephen G. Wilson, Prentice Hall, 1996.

[7] Link Analysis for the LRPT Digital Weather Satellite System, R. Dalke, R. Achatz, C. Holloway, G. Hufford, E. Quincy, National Telecommunications and Information Administration, Institute for Telecommunications Sciences, interagency document.

[8] Low Resolution Picture Transmission METOP Protocol Simulation Performance Characterization, Xuan Nguyen and Victor Sank, QSS Group Incorporated, September 11, 2001.

Acronym List

AMSU	Advanced Microwave Sounding Unit
APT	Automatic Picture Transmission
ASM	Attached Synchronization Marker
AVHRR	Advanced Very High Rate Radiometer
BER	Bit Error Rate
BPE	Bit Plane Encoder
CADU	Channel Access Data Unit
CCSDS	Consultative Committee for Space Data Systems
COTS	Commercial Off The Shelf
CPU	Central Processor Unit
CVCDU	Coded Virtual Channel Data Unit
dB	decibel
DCT	Discrete Cosine Transform
E_b/N_0	Energy per Bit /Noise
EDCT	Enhanced Discrete Cosine Transform
FIFO	First In First Out
GRAS	GNSS Receiver for Atmospheric Sounding
GSFC	Goddard Space Flight Center
HIRS	High Resolution Sounder
I/O	Input Output
ITS	Institute for Telecommunications Science
JPEG	Joint Photographic Experts Group
JSC	Johnson Space Center
KHz	Kilo Hertz
Km	Kilometer
LDS	LRPT Demonstration System
LRPT	Low Rate Picture Transmission
METOP	Meteorological Operational
MHS	Microwave Humidity Sounder
MHz	Mega Hertz
MLT	Modulated Lapped Transform
MODEM	Modulator – Demodulator
MPDU	Multiplexing Protocol Data Unit
NASA	National Aeronautics and Space Administration
NOAA	National Oceanic and Atmospheric Administration
PC	Personal Computer
PCAPDU	Physical Access Channel Protocol Data Unit
PN	Pseudo-random Noise
QPSK	Quadrature Phase Shift Keying
RAM	Random Access Memory
RF	Radio Frequency
R-S	Reed-Solomon
SEM	Spacecraft Environment Monitor
SEMCO	Systems Engineering and Management Corporation

SRRC	Square Root Raised Cosine
UW	Unique Word
VCDU	Virtual Channel Data Unit
VCDU-Id	Virtual Channel Data Unit Identifier